

Marwa M. ISMAIL¹, Taha A. ELWI², Ali J. SALIM¹

¹ University of Technology, Baghdad, Iraq

² Al-Ma'moon University College, Baghdad, Iraq

RECONFIGURABLE COMPOSITE RIGHT/LEFT-HANDED TRANSMISSION LINE ANTENNA BASED HILBERT/MINKOWSKI STEPPED IMPEDANCE RESONATOR FOR WIRELESS APPLICATIONS

The **subject matter** of the article is the analysis and design of a via free metamaterial antenna based on a composite right/left-handed transmission line (CRLH-TL) structure. The **goal** is to design a high-gain antenna with dual-band resonance capable of changing its resonance frequency and gain adaptively. The **tasks** to be solved are creating an antenna with a high gain-bandwidth product along the operated band, achieving adaptive frequency reconfiguration and creating a direct antenna modulation process using active elements. The **simulation methods** used are: the proposed antenna is designed by integrating a CRLH-TL structure to a 1D array based on two types of unit cells: The first unit cell is realized from a Hilbert curve of the 3rd order, and the second one is based on the 1st order of Minkowski – stepped impedance resonator (SIR). The antenna parts are printed on a Taconic RF-43 substrate with thickness = 1.57 mm. The following **results** were obtained: The Hilbert/Minkowski–SIR antenna achieved dual-band operation with a maximum gain equal to 14 dBi and 18 dBi at 5 GHz and 5.5 GHz, respectively. Furthermore, by changing the states of the PIN diode, an amplitude shift keying direct antenna modulation process is achieved; for instance, at 5 GHz, the antenna can change its gain directly in the range from (12-14) dBi with good impedance matching. Finally, the proposed antenna shows a low profile and operates at different frequency bands within sub-6 GHz applications. **Conclusions.** The simulation results indicate that such antenna performance enhancement is the result of eliminating via conduction losses, ground plane capacitance losses and suppressing surface wave reflections due to the Hilbert/Minkowski SIR introduction.

Keywords: Frequency reconfiguration; Hilbert; Minkowski; Metamaterial; SIR.

1. Introduction

Due to the increased demand for wireless communication systems, it has become necessary to provide small-sized and low-cost antennas, in addition to the high performance represented by multiband and high gain [1]. Recently, various methods have appeared to design miniaturized antennas through metamaterial (MTM) introduction [2]. MTM structures can be manufactured using transmission lines or resonance apertures. The transmission line approach consists of CRLH structures. In contrast, the resonant approach consists of a split-ring resonator (SRR) or a complementary split-ring resonator (CSRR). However, the MTM-compact design resulted in a narrow bandwidth, low gain, and low radiation efficiency [3], as well as the design complexity of using via, which restricts the use of metamaterials in various wireless applications [4].

1.1. Motivation

To overcome the above problems and enhance the antenna performance, various methods were used, including MTMs with the antenna structure [5], such as

electromagnetic band gap (EBG), artificial magnetic conductor (AMC) reflector, and frequency selective surface (FSS) substrates. However, these multi-layer antennas suffer from increased size, low bandwidth, low efficiency and low gain, and the presence of via complicates the antenna fabrication process [6]. Therefore, these antennas are not suitable for applications that require higher efficiency with lower complexity. These challenges represent the motivation to construct an antenna based on a single layer MTM via free structures with high gain and reconfigurable properties that meet modern wireless network requirements.

In the proposed design, pre-fractal is used as EBG inclusion due to its distinctive characteristics that provide a solution to reduce the MTM limitations mentioned above, where pre-fractals provide the following advantages:

1. The performance of impedance matching and gain is increased rapidly after introducing the pre-fractal structures; This is due to reduce the capacitive effects of the ground plane that produce losses and field cancellation. As a result, dual band at 5 and 5.5 GHz with a peak gain of 14 dBi, and 18 dBi is achieved, respectively.

2. Frequency reconfiguration with multiple bands is achieved with pre-fractal structures, where its geometrical shape and path discontinuity help extend the resonance frequency with good impedance matching. Up to five bands with moderate to high gain are achieved.

3. The design is via free, which eliminates the losses generated from using in addition to reducing its complexity.

1.2. State of the Art

CRLH-TL has been used in many applications for their properties; this section presents some current state of the art in this field.

In [7], a frequency-pattern reconfigurable antenna was designed, and the reconfiguration process was achieved using an electrical switching mechanism with four PIN diodes. The antenna operates at 2.45 GHz, 3.1 GHz, 4.1 GHz, 3.8 GHz, 7.8 GHz, and 9.5 GHz, which is suitable for various wireless applications. Furthermore, a pattern reconfigurable microstrip antenna with a dual-band operation was presented in the study [8]; the antenna operates at 2.4 GHz and 5.8 GHz with omni and directional radiation patterns, respectively. Additionally, a dual-band pattern reconfigurable antenna for beam steering applications was proposed [9]; an EBG structure was used to achieve reconfiguration at 2.45 GHz and 5.8 GHz with beam steering of (0° , $+26^\circ$, and -26°). Furthermore, a frequency-pattern reconfigurable antenna with beam steering capability was designed [10], 8 PIN diodes were used to control antenna performance, and the proposed design can operate at various sub-6 5G bands, including 2.6 GHz, 3.5 GHz, 4.2 GHz, 4.5 GHz, and 5 GHz with good gain across the operated bands. In the studies [11, 12] a phased array antenna with a CRLH phase shifter is proposed. The beam scan controlled magnetically using an integrated magnetic practice; this reduces the complexity of the biasing system and is very useful in MIMO systems; however, the magnetic control mechanism is under study, and its characteristics are not fully controlled.

Furthermore, an optimization technique for radar cross section (RCS) estimation in a planar antenna array is presented in [13]. The results show the ability of the proposed technique to enhance the scatterometric radar requirements associated with planar-phased antenna arrays. Finally, a simulation study is presented in [14], take into account different dielectric substrates and various patch shapes where the design parameters are changed, and their effect is studied in each case.

From the above research [7–10], the antenna suffers from low to moderate gain arising from the capacitive effect of the ground plane in addition to using via [9] that produces losses and affects the radiation pattern. To eliminate the losses resulting from such a technology, it has

become necessary to present new designs that reduce these losses; This is the focus of this research.

1.3. Objective

This research introduces an MTM-TL antenna with a new structure to achieve high gain and efficiency at the operating frequency bands. The proposed design consists of an asymmetric T-shaped CRLH unit cell structure as an interdigital capacitor (C_{IDC}) coupled to a T-stub inductor (L_{TS}) to realize gain-bandwidth product enhancement. Additionally, nine-unit cells of the Hilbert curve are interlocked with eight Minkowski-SIR unit cells on the substrate backside to avoid via losses. Thus, the total number of the CRLH-TL is seventeen-unit cells fed with an asymmetric coplanar waveguide (CPW). As a result, the proposed antenna shows dual frequency bands of operation with a gain of 14 dBi and 18 dBi at 5 and 5.5 GHz, respectively.

This paper is organized as follows: First, the Hilbert/Minkowski SIR antenna design and all geometrical details are discussed. Next, a parametric study is discussed, and the effects of the antenna dimension variation on the relative performance are analyzed in detail. Next, a frequency reconfiguration is discussed. Next, a comparison between the proposed antenna performances with the latest relative research activities is discussed. Finally, the conclusion is followed later.

2. Antenna Design Based on Hilbert/Minkowski SIR Structure

The CRLH unit cell is presented in Fig. 1; the unit cell consists of an interdigital capacitor C_{IDC} in series with a stub inductor L_{TS} . This series produces the LH branch, while the parasitic effects realize the RH branch, reducing the antenna efficiency. Thus, a structure based on a 3rd-order Hilbert unit cell is introduced to eliminate the impact of RH branches incorporated with a 1st-order Minkowski-SIR cells. Such introductions amplify the magnetic field effects, which increases the displacement current flow toward the unit cell and thus enhances the antenna performance. The CRLH structure was fed by an asymmetric CPW feeding technique where the ground plane dimensions differed on both sides of the feeding structure. Taconic RF-43 substrate with $\epsilon_r = 4.3$ and thickness = 1.57 mm was used for the design. The CRLH unit cell is attached to a rectangular pad, as seen in Fig. 1, d. One PIN diode is inserted in each pad to control the antenna performance by changing the applied bias voltage; as a result, the plasmonic surface current fluctuations on the metamaterial surface are changed, which results in shifting the resonance frequency and producing multiple bands suitable for various applications. The following sections provide extra details about the other antenna parts.

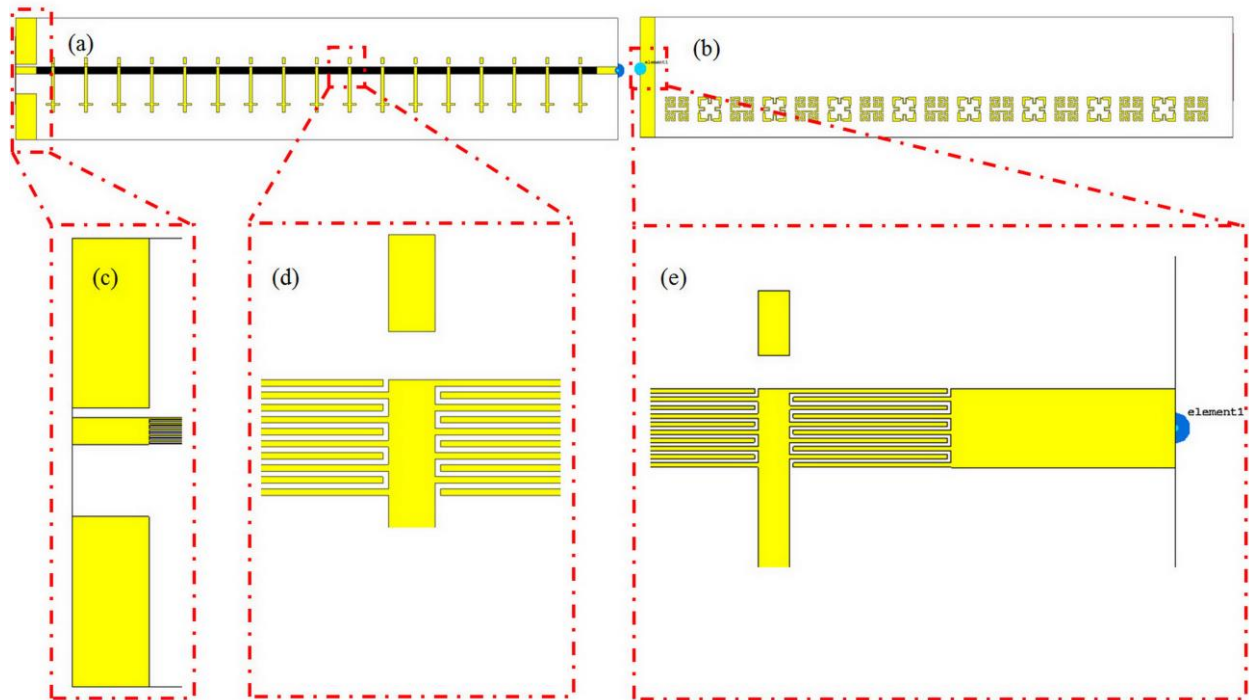


Fig. 1. Antenna geometrical details: (a) – top-view, (b) – back-view, (c) – coplanar waveguide feeding structure, (d) – rectangular pad, (e) – matching impedance

2.1. CRLH-MTM Unit Cell

The CRLH-TL antenna is fed with an asymmetric CPW feeding structure where the ground plane dimensions differ on both sides of the CPW feeding technique. The proposed CRLH-TL antenna consists of an interdigital capacitor based on five fingers on each side that acts as a series capacitor. The proposed T-stub inductor represents a shunt inductor combined with the capacitor to produce the LH branch, as seen in Fig. 2. The ground plane stores energy, representing an interactive (capacitive effect) [15]; Hilbert/Minkowski SIR inclusions are printed on the substrate backside to eliminate the ground plane reflected energy with minimum conduction loss, thus reducing the losses and balancing the capacitive effects. However, the conductive and dielectric parts create the parasitic effects of the RH branch, which limits the antenna performance.

Additionally, the ground plane, represented by a layer of copper, acts as a reflector [16], reflecting the signal with a phase opposite to that of the source wave. Generally, the source wave represents the wave flowing along the radiator; the reflected wave differs in phase from the source wave, resulting in destructive interference with the source wave. This interference cancels out the main wave or limits significantly, which reduces the radiation efficiency; as a result, gain decreases due to miss-matching caused by field cancelation. These unwanted effects are minimized by placing the ground plane at $\lambda/4$ from the radiator [17], as shown in Fig. 3.

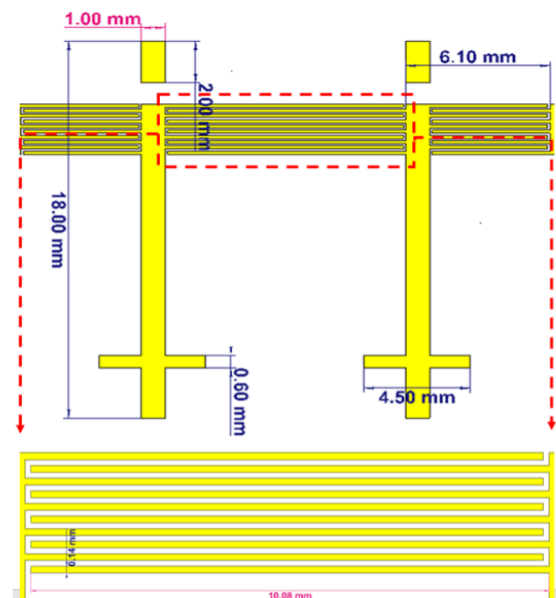


Fig. 2. CRLH cell dimensions

In the proposed design, the Hilbert/Minkowski SIR unit cells replaced the ground layer, and thus the losses caused by the ground plane are significantly reduced; This can be understood from the surface current distribution, first with the ground plane and second with the proposed SIR structure, as shown in Fig. 4, a,b. The proposed SIR structure reduces the back reradiation and reflections caused by the ground plane, which results in better current distributions and hence better matching and radiation pattern.

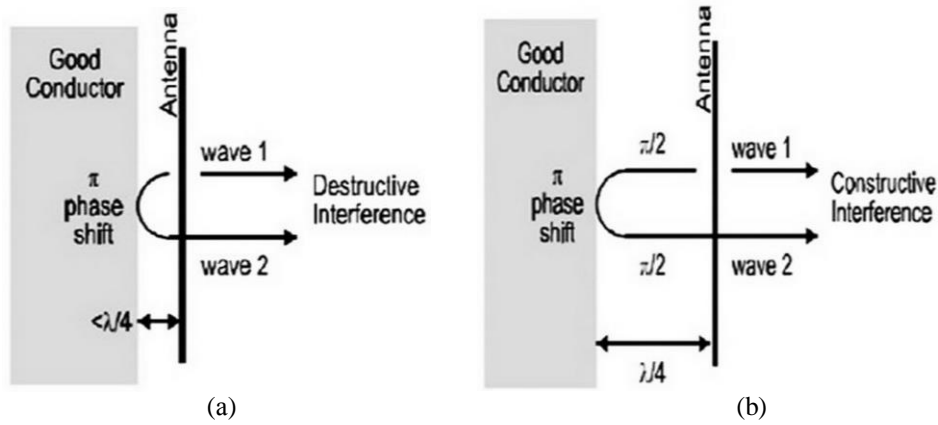


Fig. 3. Antenna separation: (a) closed, (b) at $\lambda/4$ from the ground plane

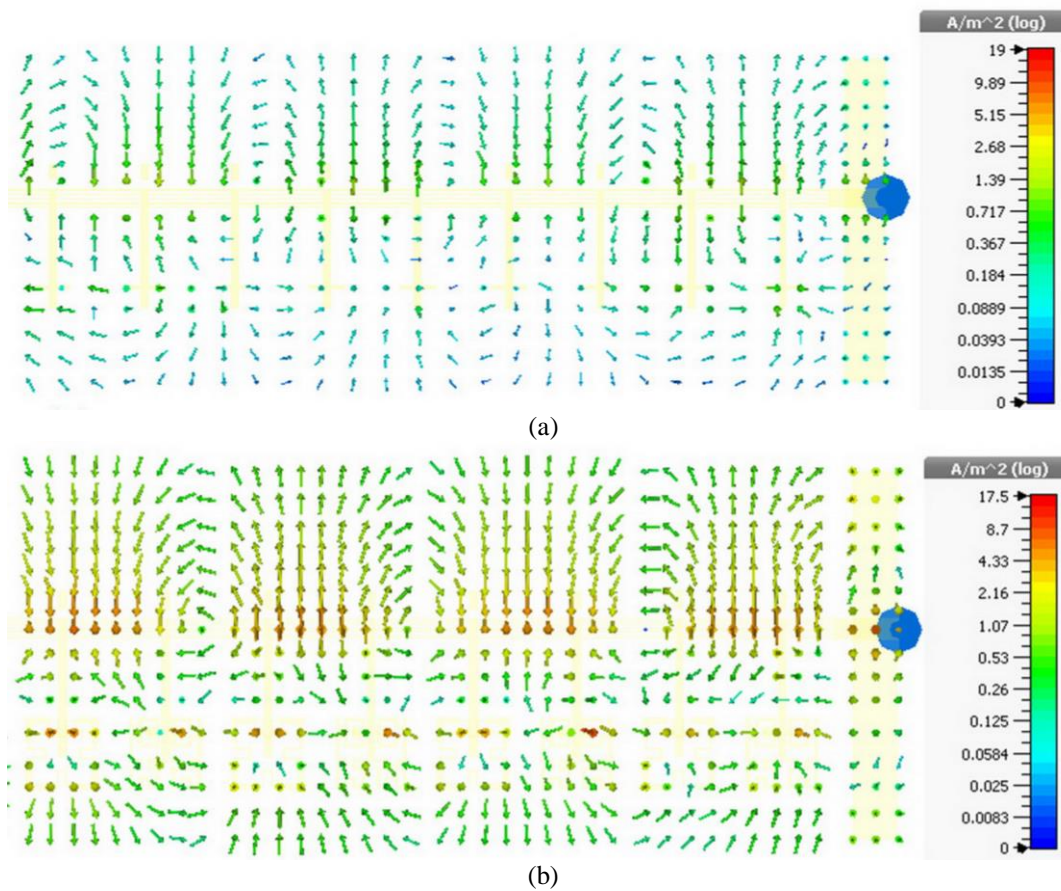


Fig. 4. Surface current density: (a) without SIR structures, (b) with SIR structures

2.2. SIR Structure

SIR structures can be periodic or semi-periodic arrays printed on dielectric materials [18]. They have been used for their distinctive properties in reducing surface waves in many applications to improve general performance. In this design, the proposed MTM array consists of two types of unit cells, as shown in Fig. 5. The first type corresponds to nine-unit cells of the Hilbert curve printed on an area of 8 mm² from the substrate back

panel; the second type fills the space between the cells of the first array with eight-unit cells of an area of 8 mm² each.

A capacitive gap is created between array adjacent cells, and is given by the following relationship [19]:

$$c = \frac{p\epsilon_0(1+\epsilon_r)}{\pi} \cosh^{-1}\left(\frac{p+g}{g}\right), \tag{1}$$

where p is each SIR width, and g is the gap between SIR cells.

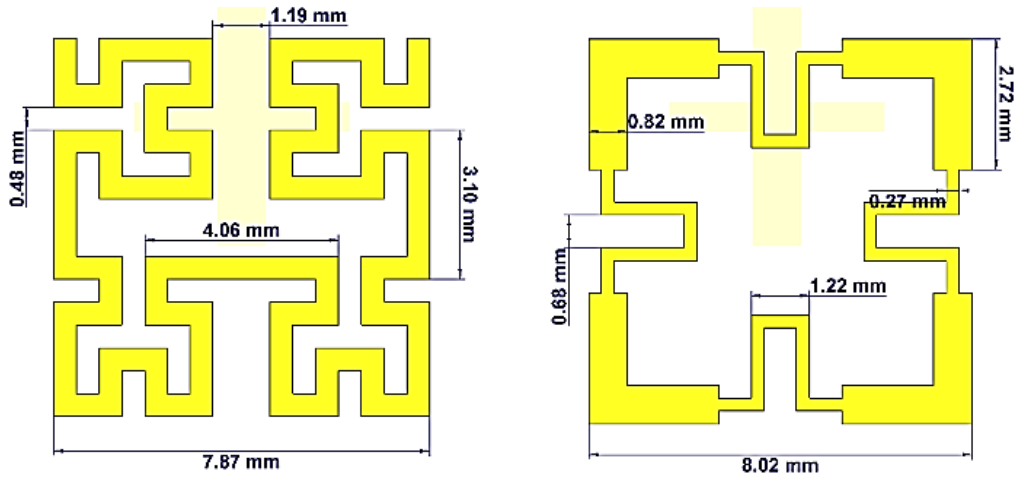


Fig. 5. Hilbert/Minkowski SIR curve dimension

The proposed SIR structures show their capacitive behavior by acting as a high-pass filter that allows the high frequencies to pass through and suppresses the low ones [20]. Note that the capacitive effect is equal on both sides of the cell because the cell is balanced according to the length of the stub. Therefore, the capacitive reactance of adjacent cells has an equal impact on suppressing surface currents, which is given by the following relationship:

$$X_c = \frac{1}{2\pi f c} . \quad (2)$$

3. Parametric Study

This section analyses the design process and examines the fundamental parameters used to achieve the final design. The simulation evidence indicates that such antenna performance enhancement is due to eliminating via conduction losses, ground plane capacitance losses, and surface wave suppression due to the Hilbert/Minkowski SIR introduction. These operations are explained as follows:

3.1. C_{IDC} influence

A detailed study was performed on the influence of fingers number on antenna performance. First, the finger number is changed from 1 to 5 to monitor the gain spectra and S_{11} variation. It is found that by increasing the number of fingers, a significant reduction in the storing losses is attributed to the structure by equalizing the capacitive reactance to the inductive reactance within the circuit, which results in better impedance matching. However, the antenna gain does not affected by the increase in finger number; this is due to the insignificant electric current gradient on the miniaturized unit cell, as seen in Fig. 6.

3.2. L_{TS} Effects

The proposed T-stub dimensions have been changed to clarify the impact of L_{TS} dimensions on the antenna design; the inductor length is increased from 12 mm to 18 mm. As a result, it was found that the proposed antenna gain increased from 6.69 dBi to 8.8 dBi at 5.4 GHz. Additionally, the proposed T-shaped component at the end of the inductor acts as a small patch that helps distribute the electric current with high energy, thus, increasing the gain to reach a maximum value of 9.5 dBi for 2-CRLH unit cells, see Fig. 7.

3.3. CRLH Unit Cell

The proposed CRLH unit cell can be decomposed into four parts representing a model. For example, model 1 represents the transmission line TL only. Model 2 is based on TL and C_{IDC} . Model 3 is realized based on TL, C_{IDC} , and L_{TS} , where the proposed T-stub acts as a capacitive tuner. Finally, model 4 is the proposed unit cell of the Hilbert/Minkowski SIR structure, as seen in Fig. 8. The evaluated S_{11} and realized gain are calculated for each model, as shown in Fig. 9. A considerable reduction in the cell size is observed after the introduction of the Hilbert/Minkowski SIR structure through the shift of the second frequency resonance from 5.5 GHz to 2.9 GHz. An equivalent circuit model for the proposed unit cell using PathWave ADS 2019 software is given in Fig. 10 with S_{11} ; a good agreement is obtained between CST Studio Suite 2017 and ADS results.

3.4. Antenna Array with And Without SIR

The proposed SIR results from creating an array with two types of pre-fractals. First, the Minkowski SIR structure is inspired by [21] to obtain a dual band using a single resonator. This structure was constructed in two

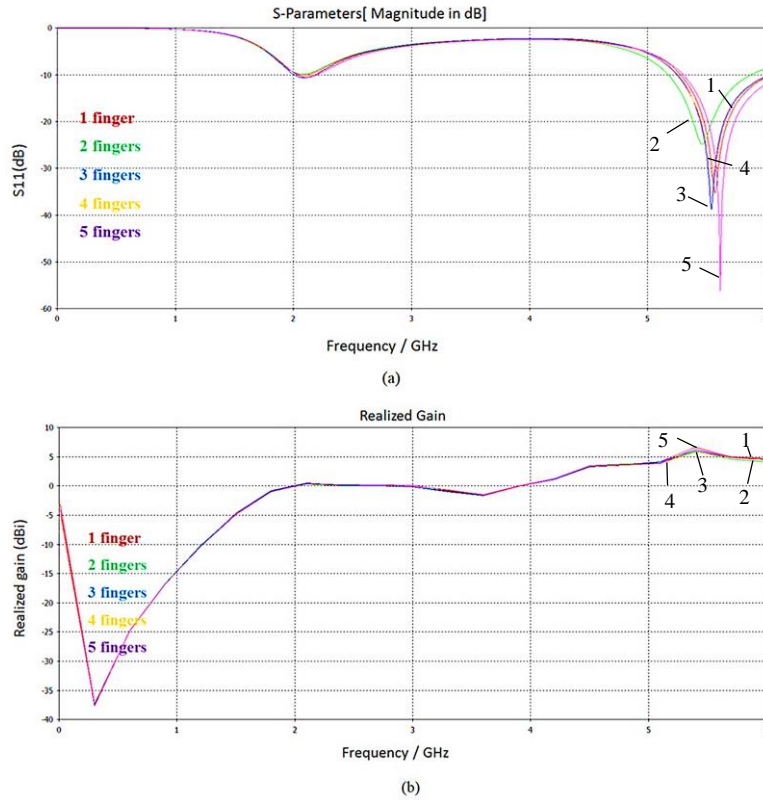


Fig. 6. C_{IDC} effects: (a) – S₁₁, (b) – realized gain

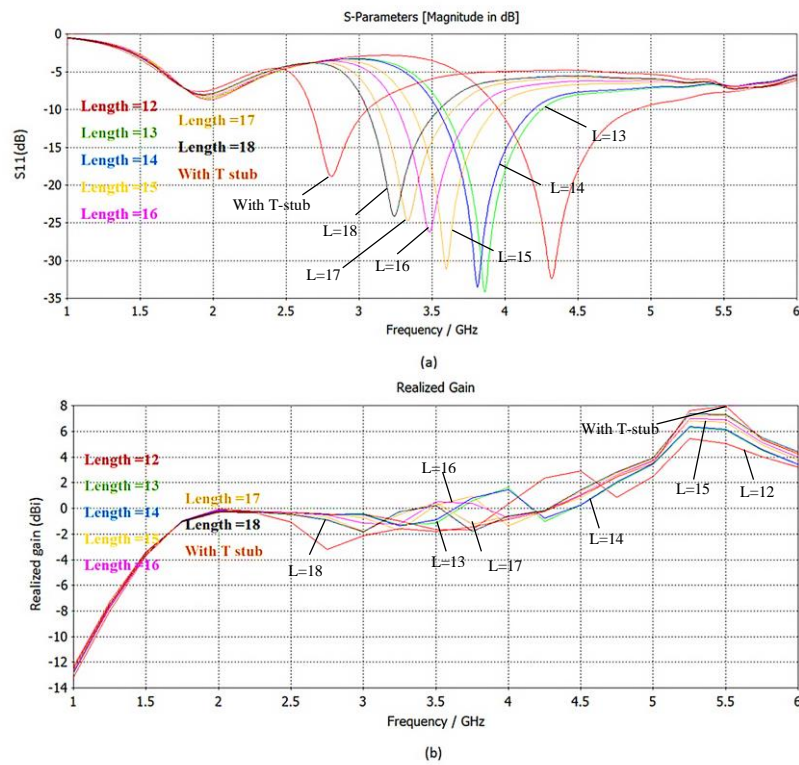


Fig. 7. L_{TS} effects: (a) – S₁₁, (b) – realized gain

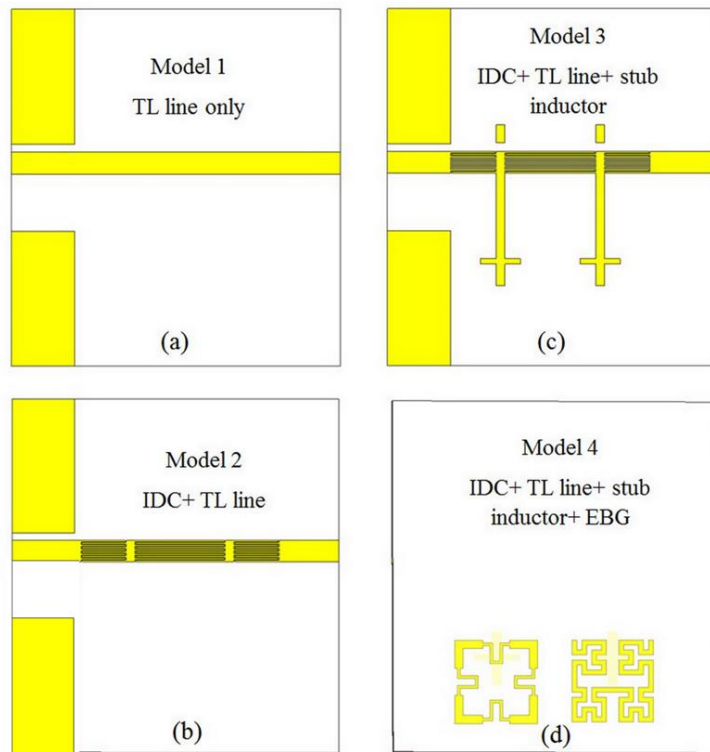


Fig. 8. CRLH-unit cell: (a) – Model 1, (b) – Model 2, (c) – Model 3, (d) – Model 4

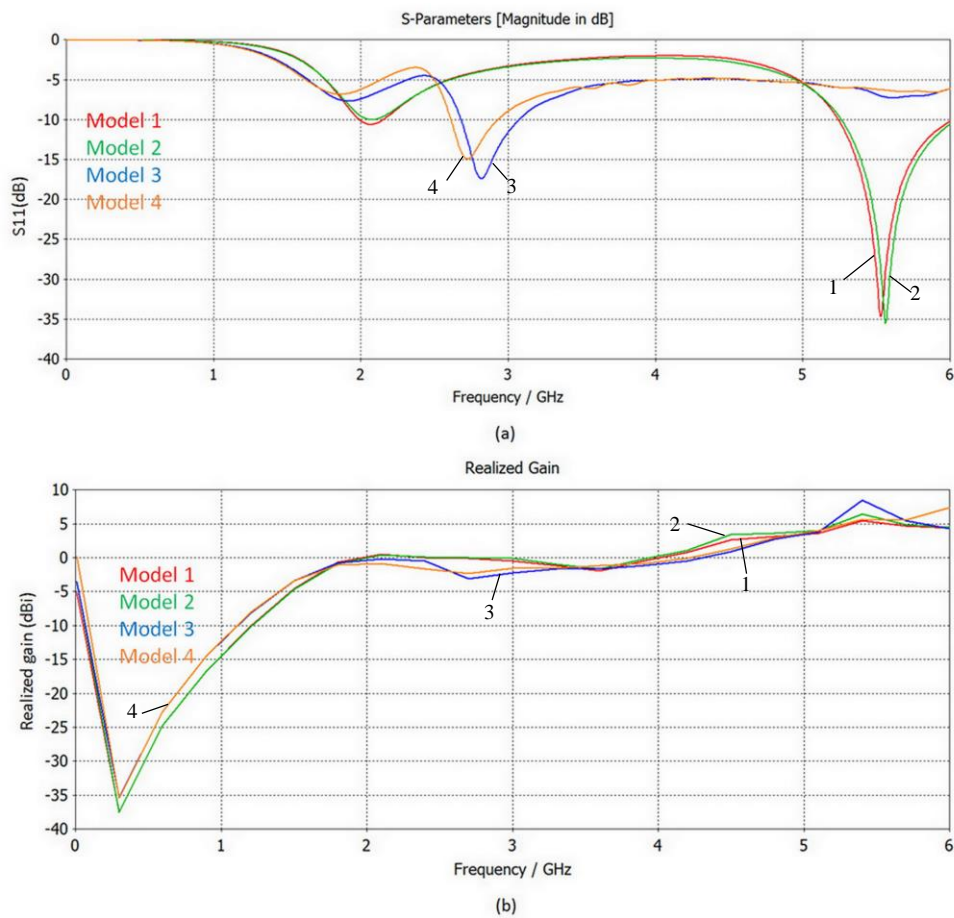


Fig. 9. CRLH-unit cell parametric study: (a) – S_{11} , (b) – realized gain

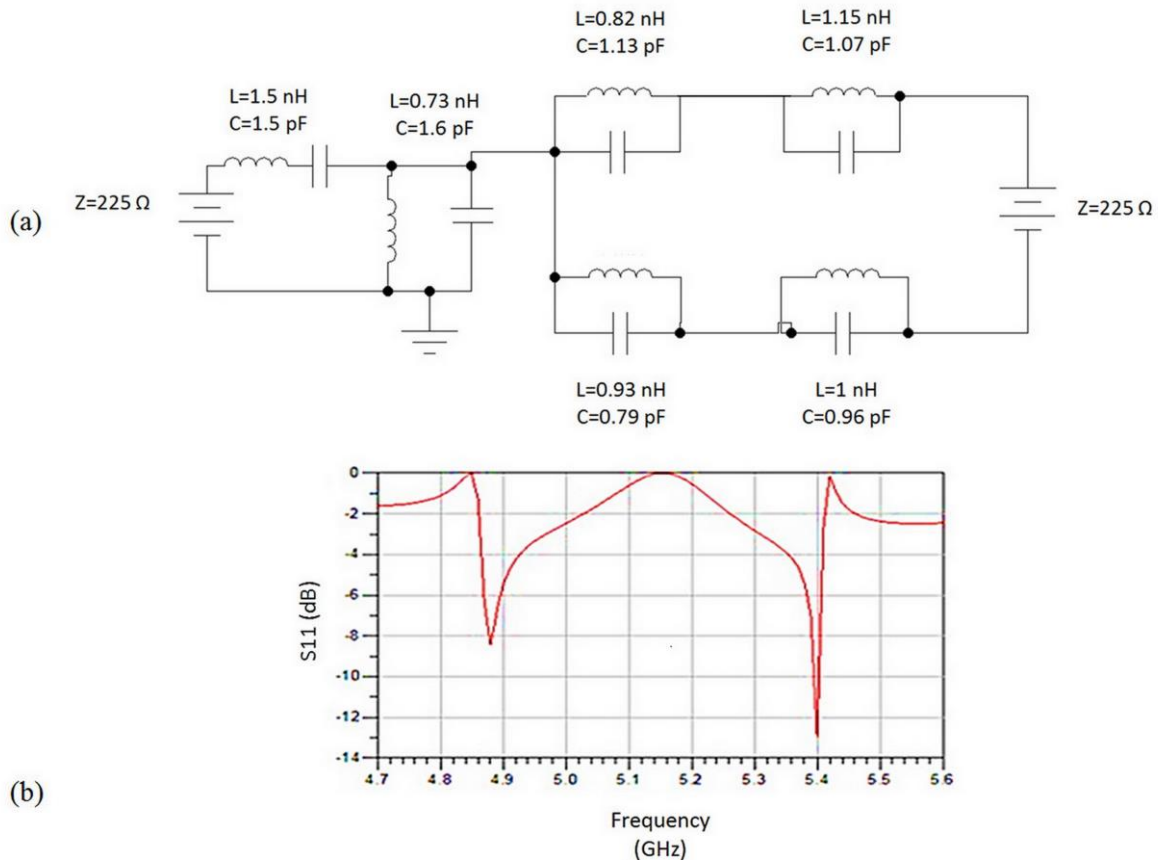


Fig. 10. ADS results: (a) – ADS equivalent circuit, (b) – S_{11}

steps; the SIR technique was first added to all sides of a square loop resonator. Next, 1st-order Minkowski pre-fractal curves were added. Finally, this pre-fractal was combined with the Hilbert curve to create the proposed SIR defects.

This section studied the effect of MTM SIR structure on antenna performance. Two cases were taken: one with SIR defects and the second with the absence of SIR defects. As a result, the resonance frequency is shifted with better matching, resulting in higher performance. Furthermore, the gain reached the highest value at 5.5 GHz with 16 dBi and 13.3 dBi at 5 GHz; this is due to the introduction of SIR structure that reduces the surface waves resulting in better gain and S_{11} , as shown in Fig. 11. Fig. 12 shows the radiation pattern in each mode. It is good to note that the proposed design shows two main lobes at 5.5 GHz by splitting the main beam into two lobes. This feature is desirable in many 5G system applications to track more than one object simultaneously in orthogonal frequency-division multiplexing (OFDM) algorithms [22-24].

3.5. SIR Defects study

Finally, to clarify the effect of increasing the number of SIR rows on antenna performance, the number of rows was increased from one to three, and a comparison

is made in terms of S_{11} and gains spectra. It is observed that when the number of rows increases, the number of modes increases; this is due to the path discontinuity offered by each SIR unit cell, in addition to a noticeable decrease in antenna gain due to the storing losses caused by the SIR cells, which decrease the antenna efficiency. Depending on this fact, one row is used as the basis for the antenna design, see Fig. 13.

4. Frequency Reconfiguration

Metamaterials consist of resonant structures whose behavior varies according to the resonant frequency. They are characterized by negative constitutive parameters at frequencies lower than the resonant frequency and positive constitutive parameters at frequencies above the resonant frequency. This feature presents a drawback since most wireless applications must have fixed and unchanging working frequencies. To obtain a multi-characteristic antenna capable of working in different wireless applications and at different frequencies. The antenna must be reconfigurable, where the operating frequency is controlled by changing the applied voltage. In this design, T-symmetric CRLH -unit cells are periodically used to create the metasurface, a gap is inserted in each unit cell, and one pin diode is placed at each gap for frequency reconfigurability, see Fig. 14.

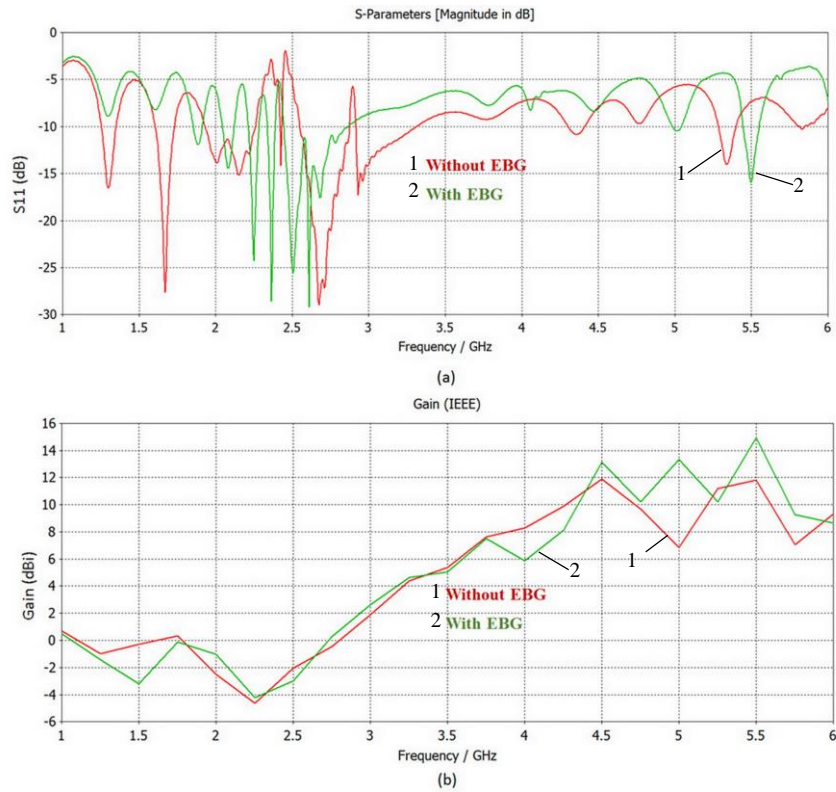


Fig. 11. SIR defect parametric study: (a) – S_{11} , (b) – gain

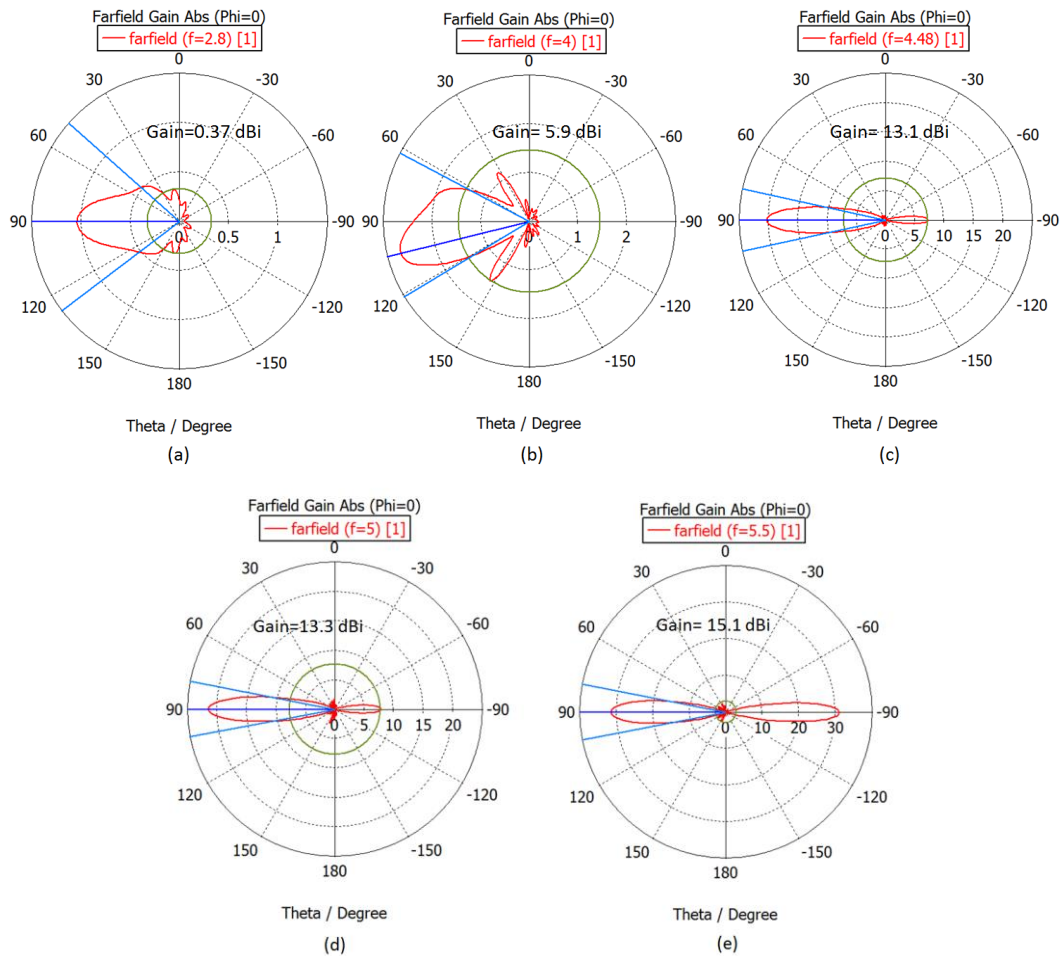


Fig. 12. Antenna radiation pattern: (a) at 2.8 GHz, (b) at 4 GHz, (c) at 4.48 GHz, (d) at 5GHz, (e) at 5.5 GHz

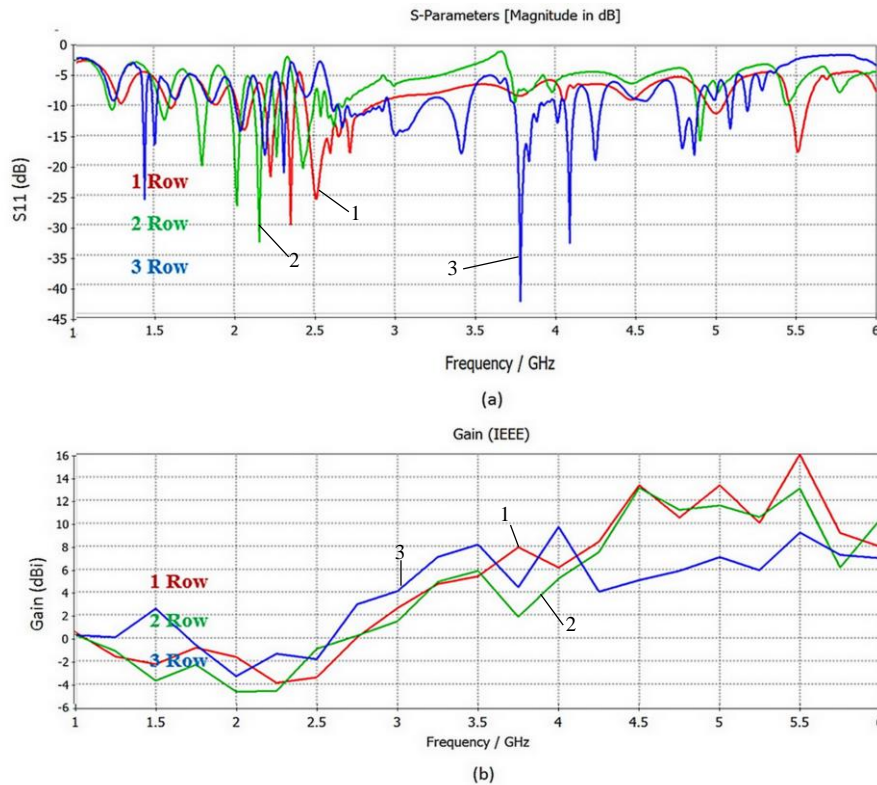


Fig. 13. Increase SIR defects study: (a) – S_{11} , (b) – gain

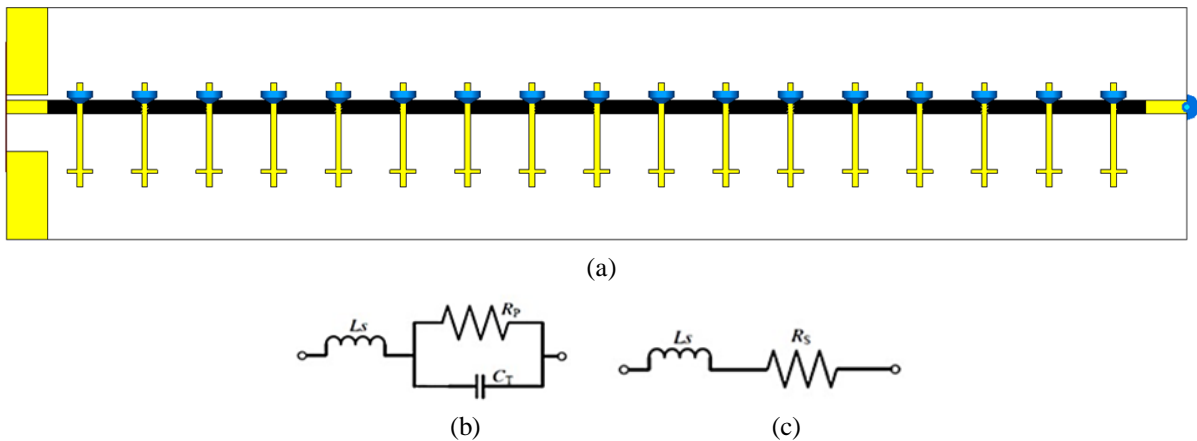


Fig. 14. Antenna structure: (a) front view, (b) equivalent circuit model of the PIN diode OFF-state, (c) ON-state

Different bands at different frequencies can be obtained by changing the input sequence of the PIN diode. Table 1 shows the input sequence of the diode, the corresponding operating frequency, and the number of created bands.

For the given cases of the input sequences, the gain and S_{11} are calculated. The array gain reached a maximum value (Table 2) with gain equal to 18 dBi at 5.5 GHz and 14 dBi at 5 GHz. It is good to mention that the proposed antenna shows a noticeable change in the evaluated gain spectra at 5 GHz and 5.5 GHz, as seen later in Fig. 15 and summarized in Table 2. These variations make the antenna a perfect candidate for direct amplitude antenna modulation.

Table 1

Frequency Reconfiguration

Antenna characteristic		
Input sequence (cases)	Number of bands	Resonance frequency, GHz
0000000000000000	2	5, 5.5
1111111100000000	5	4, 4.4, 4.9, 5.4, 5.9
1100000000000000	4	4, 4.5, 5, 5.6
1111111111111111	3	4.8, 5.3, 5.7
11111111001011011	3	4.5, 5.4, 5.8

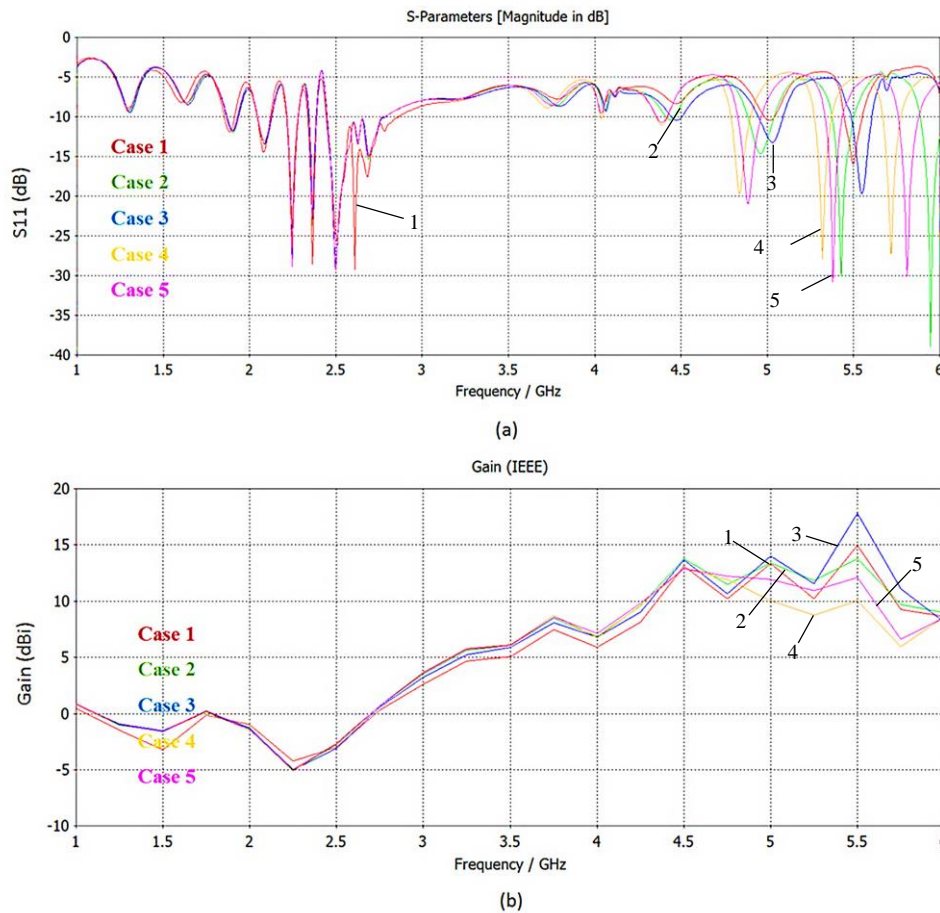


Fig. 15. Frequency reconfigurable antenna parameters for the different cases (see Tab. 1): (a) – S_{11} , (b) – gain

Direct Antenna Modulation

Input sequence (cases)	5 GHz		5.5 GHz	
	S_{11} , dB	Gain, dBi	S_{11} , dB	Gain, dBi
000000000000000000	-11	13	-18	16
111000000000000000	-13	14	-32	17.4
111111110000000000	-13	13.4	-12	14.5
000000000001111111	-10	12	-13	15

5. Comparison with The Latest Research

A comparison with the field of interest is summarized and presented in Table 3. In [25], the researcher used a PIN diode on the ground plane to reduce the reflections to the main radiator. The researcher also reduced the ground plane area to enhance the antenna gain. In [26], the researcher used eight cross slots to produce four beams simultaneously, in addition to an electrical switching mechanism to control beam steering. In [27], an array of patches with superstrate enhanced the

Table 2

overall performance, and 2 PIN diodes were used to achieve polarization reconfiguration. In [28], truncated square patches with 16 PIN diodes were used to achieve polarization reconfiguration. It is obvious from the comparison that the proposed design achieves the highest gain with good impedance matching across the operating bands, in addition to the capability of reconfiguration and amplitude shift keying (ASK) direct antenna modulation process that suits the current state of the art.

6. Discussion

In this section, the effect of each part of the design is explained briefly and sequentially, as given by the parametric study:

- C_{IDC} effect:- the storing losses are equalized by adding the C_{IDC} to the design. This can be understood from the increase in impedance matching with increasing the number of fingers, as shown in Fig. 6;
- T-stub effect:- the T-stub equalizes the capacitive effect and reduces the storing losses, which resulted

Table 3

Comparison with the latest research

Ref	Freq. GHz	Reconfig. Type	Technique used	gain dBi	Switching type	Design type / size mm ²
[4]	3.3-4.2, 4.86-5.98	Frequency + continuous scanning	CRLH/ Hilbert EBG defects	3.74/ 7.24	Electrical (17 PIN)	Array / 40*240
[7]	3.1, 4.1, 3.8, 2.45, 7.8, 9.5	Frequency/ pattern	Hexagon shape-patch-CPW	4.24	Electrical (2 PIN)	Single element / 30 × 20
[8]	2-3, 5.2-6.6	Frequency	Slots	-10	Electrical (2 PIN)	Single element/ 30*35
[9]	2.4 & 5.8	Pattern	EBG structure	Simulation (5.52 /6.66 6.66/ 6.73) Measured (3.53/ 3.24 3.26/ 3.59)	Electrical (14 PIN)	Single element/ 113*113
[10]	2.6, 3.5, 4.2, 4.5, and 5, 5.5	Frequency/ pattern	parasitic patches	1.72/1.94/2.51/2.81/3.66/3.8	Electrical (8 PIN)	Single element/ 31 * 27
[25]	4.66, 5.2, 5.3, 5.8	frequency	V-Shape microstrip	6	Electrical (2 PIN)	Single element/ 16 * 16
[26]	5.8	Pattern	Slots	4.33	Electrical (2 PIN)	Single element
[27]	5.8	Polarisation	superstrate/array of patches	3.7	Electrical (2 PIN)	Array/ 84*50
[28]	5.8	Polarisation	truncated square patch	11.9	Electrical (16 PIN)	Array/ 70*70
[30]	4.8 to 6	Polarisation	truncated patch/ metasurface	7.3	Electrical (2 PIN)	Single element/ 48*48
[32]	2.32 3.5	Frequency	ACS-FED Asymmetric coplanar strip-fed	0.69 / 1.278	Electrical (1 PIN)	16.5* 10.5
This work	5, 5.5	frequency	CRLH/ Hilbert/ Minkowski – SIR EBG inclusion z	14/18	Electrical (17 PIN)	Array / 40*240

– in an increase in antenna gain from 6.69 to 8.8 dBi at 5.4 GHz, the cross shape patch at the end of the inductor increases the current distribution with good energy that maximize the gain to 9.5 dBi, as seen in Fig. 7;

– to build the equivalent circuit model for the proposed design and extract the L-C parameters that provide the resonance frequency. The circuit model for the CRLH antenna is designed using ADS 2019 software tool; An excellent agreement is found in S₁₁ results between the CST software tool and AD, as seen in Fig. 10;

– SIR effect:- adding the SIR as inclusion replaces the ground plane and reduces its storing losses, thus resulting in better matching and gain. The gain reaches a peak value of 16 dBi at 5.5 GHz and 13.3 dBi at 5 GHz, as seen in Fig. 11. However, an increase in the number of EBG rows increased the number of modes; as a result, reducing the overall gain, thus one row is selected for the design, as shown in Fig. 13;

– by changing the PIN input sequence; the surface current distribution can be changed, which affects the overall performance. As a result, various resonance frequencies can be obtained with good gain and impedance

matching, as shown in Fig. 15. It is good to note that various gain values are obtained at 5.5 GHz, which candidate the antenna for ASK direct modulation, as seen in Fig. 15, b.

7. Conclusion

A pre-fractal-MTM -via a free antenna is proposed in this paper. The antenna is organized by loading 17 unit cells of the Hilbert/Minkowski SIR curve on the CRLH-MTM structure. The design occupies an area of 40*200 mm² and is printed on a Taconic FR-4 substrate. The antenna performance is controlled using an electrical switching technique, where the antenna characteristics can be changed according to the bias voltage. Furthermore, the ground plane creates a capacitive effect, resulting in losses and reducing the antenna efficiency. Therefore, EBG inclusion is used to replace the ground plane and minimize its effect. Additionally, the pre-fractal structures help in providing multiple bands with good matching due to their path discontinuity as a result. It is found that the proposed antenna has a dual-band operation at 5 GHz and 5.5 GHz with a peak gain of 14 dBi and 18 dBi, respectively. Finally, the equivalent circuit model using ADS software was built and compared to the CST; a good agreement was obtained between the results. Therefore, the proposed design can be used in various wireless applications. Finally, increasing the antenna efficiency and reducing the bias complexity is one of the research concerns that should be considered in future research. Therefore, using an alternative tool to control antenna performance without bias wires becomes an urgent need. For future work:- Methods of magnetic control and optical control will be selected to reduce biasing circuits.

Contribution of authors: development of theoretical formalism and performance of numerical simulations – **Marwa M. Ismail**; the final version of the manuscript – **Marwa M. Ismail** and **Taha A. Elwi**; project management – **Taha A. Elwi** and **Ali J. Salim**.

References

1. Ahmed, H. S., Ali, J. K. and Salim, A. J. Design of fractal-based bandstop filter for microwave radiation leakage reduction. *Engineering and Technology Journal*, 2017, vol. 35, iss. 1, pp. 16-23. DOI: 10.30684/etj.2017.127306.
2. Karimbu Vallappil, A., A. Rahim, M.K., A. Khawaja, B., Iqbal, M.N., Murad, N.A., Gajibo, M.M., O. Nur, L. and S. Nugroho, B. Complementary split-ring resonator and strip-gap based metamaterial fractal antenna with miniature size and enhanced bandwidth for 5G applications. *Journal of Electromagnetic Waves and Applications*, 2022, vol. 36, iss. 6, pp. 787-803. DOI: 10.1080/09205071.2021.1983878.
3. Singh, M., Kumar, N., Dwari, S., Parthasarathy, H. and Kala, P. A compact dual-band zeroth-order resonator antenna loaded with meander line inductor. *International Journal of RF and Microwave Computer-Aided Engineering*, 2020, vol. 30, iss. 7, article no. e22231. DOI: 10.1002/mmce.22231.
4. Ismail, M. M., Elwi, T. A. and Salim, A. J. A Miniaturized Printed Circuit CRLH Antenna-based Hilbert Metamaterial Array. *Journal of Communications Software and Systems*, 2022, vol. 18, iss. 3, pp. 236-243. DOI: 10.24138/jcomss-2022-0030.
5. Rasool, J. M. MIMO Antenna System Using Orthogonally Polarized Ultra Wide Band Antennas With Metamaterial. *Engineering and Technology Journal*, 2010, vol. 28, iss. 24, pp. 6845-6853. DOI: 10.30684/etj.28.24.2.
6. Ameen, M., Mishra, A. and Chaudhary, R. K. Dual-band CRLH-TL inspired antenna loaded with metasurface for airborne applications. *Microwave and Optical Technology Letters*, 2021, vol. 63, iss. 4, pp. 1249-1256. DOI: 10.1002/mop.32725.
7. Ullah, S., Elfergani, I., Ahmad, I., Din, I. U., Ullah, S., Rehman Khan, W. U., Ahmad, T., Habib, U., Zebiri, C. and Rodriguez, J. A Compact Frequency and Radiation Reconfigurable Antenna for 5G and Multistandard Sub-6 GHz Wireless Applications. *Wireless Communications and Mobile Computing*, 2022, vol. 2022, article id: 4658082. DOI: 10.1155/2022/4658082.
8. Al-Saeedi, M. M., Hashim, A. A., Al-Bayati, O. H., Rasheed, A. S. and Finjan, R. H. Design of dual band slotted reconfigurable antenna using electronic switching circuit. *Indonesian Journal of Electrical Engineering and Computer Science*, 2021, vol. 24, iss. 1, pp. 386-393. DOI: 10.11591/ijeecs.v24.i1.pp386-393.
9. Ismail, M. F., Rahim, M. K. A., Hamid, M. R., Majid, H. A., Omar, A. H., Nur, L. O. and Nugroho, B. S. Dual-band pattern reconfigurable antenna using electromagnetic band-gap structure. *AEU - International Journal of Electronics and Communications*, 2021, vol. 130, article id: 153571. DOI: 10.1016/j.aeue.2020.153571.
10. Ahmad, I., Dildar, H., Khan, W. U. R., Shah, S. A. A., Ullah, S., Ullah, S., Umar, S. M., Albreem, M. A., Alsharif, M. H. and Vasudevan, K. Design and Experimental Analysis of Multiband Compound Reconfigurable 5G Antenna for Sub-6 GHz Wireless Applications. *Wireless Communications and Mobile Computing*, 2021, vol. 2021, article id: 5588105. DOI: 10.1155/2021/5588105.
11. Ayaz, M., & Ullah, I. A Phased Array Antenna with Novel Composite Right/Left-Handed (CRLH) Phase Shifters for Wi-Fi 6 Communication Systems. *Applied Sciences*, 2023, vol. 13, iss. 4, article id: 2085.

DOI: 10.3390/app13042085.

12. Ayaz, M., Iftikhar, A., Braaten, B. D., Khalil, W., & Ullah, I. A Composite Right/Left-Handed Phase Shifter-Based Cylindrical Phased Array with Reinforced Particles Responsive to Magneto-Static Fields. *Electronics*, 2023, vol. 12, iss. 2, article id: 306. DOI: 10.3390/electronics12020306.

13. Volosyuk, V., Zhyla, S., Pavlikov, V., Vlasenko, D., Kosharskiy, V., Kolesnikov, D., Inkarbaeva, O. and Nezhalskaya, K. Optimal radar cross section estimation in synthetic aperture radar with planar antenna array. *Radioelectronic and Computer Systems*, 2021, no. 1, pp. 50-59. DOI: 10.32620/reks.2021.1.04.

14. Pandya, P. R., Saradadevi, M. and Langhnoja, N. Empirical analysis of microstrip patch antenna for different substrate materials and shapes using aperture coupled technique. *Radioelectronic and Computer Systems*, 2022, no. 1, pp. 170-177. DOI: 10.32620/reks.2022.1.13.

15. de Dieu Ntawangaheza, J., Sun, L., Li, Y. and Xie, Z. Improving Bandwidth, Gain and Aperture Efficiency of Patch Antenna Using Hybrid AMC Ground Plane. *Progress In Electromagnetics Research C*, 2020, vol. 103, pp. 71-82. DOI: 10.2528/PIERC20030903.

16. Dash, S. K. K., Khan, T., Kanaujia, B. K. and Antar, Y. M. Gain improvement of cylindrical dielectric resonator antenna using flat reflector plane: a new approach. *IET Microwaves, Antennas & Propagation*, 2017, vol. 11, iss. 11, pp. 1622-1628. DOI: 10.1049/iet-map.2017.0284.

17. Kaur, H., Singh, H. S. and Upadhyay, R. A compact dual-polarized co-radiator MIMO antenna for UWB applications. *International Journal of Microwave and Wireless Technologies*, 2022, vol. 14, iss. 2, pp. 225-238. DOI: 10.1017/S1759078721000349.

18. Ali, J.K., Abdul-Baki, E.M. and Hamed, M. H. A multiband fractal dipole antenna for wireless communication applications. *Engineering and Technology Journal*, 2010, vol. 28, iss. 10, pp. 2043-2053. DOI: 10.30684/etj.28.10.15.

19. Bhavarthe, P. P., Rathod, S. S. and Reddy, K. T. A compact two via slot-type electromagnetic bandgap structure. *IEEE Microwave and Wireless Components Letters*, 2017, vol. 27, iss. 5, pp. 446-448. DOI: 10.1109/LMWC.2017.2690822.

20. Maximo-Gutierrez, C., Hinojosa, J., Martínez-Viviente, F.L. and Alvarez-Melcon, A. Design of high-performance microstrip and coplanar low-pass filters based on electromagnetic bandgap (EBG) structures. *AEU - International Journal of Electronics and Communications*, 2020, vol. 123, article id: 153311. DOI: 10.1016/j.aeue.2020.153311.

21. Ziboon, H. T. and Ali, J. K. Compact quad-band BPF design with fractal stepped-impedance ring

resonator. *ARPJ Journal of Engineering and Applied Sciences*, 2017, vol. 12, iss. 24, pp. 7352-7363.

22. Zhang, R., Hao, W., Sun, G. and Yang, S. Hybrid precoding design for wideband THz massive MIMO-OFDM systems with beam squint. *IEEE Systems Journal*, 2020, vol. 15, iss. 3, pp. 3925-3928. DOI: 10.1109/JSYST.2020.3003908.

23. Pavlikov, V., Belousov, K., Zhyla, S., Tserne, E., Shmatko, O., Sobkolov, A., Vlasenko, D., Kosharskiy, V., Odokiienko, O. and Ruzhentsev, M. Radar imaging complex with sar and asr for aerospace vehicle. *Radioelectronic and Computer Systems*, 2021, no. 3, pp. 63-78. DOI: 10.32620/reks.2021.3.06.

24. Volosyuk, V., Zhyla, S., Pavlikov, V., Tserne, E., Sobkolov, A., Shmatko, O. and Belousov, K. Mathematical description of imaging processes in ultra-wideband active aperture synthesis systems using stochastic sounding signals. *Radioelectronic and Computer Systems*, 2021, no. 4, pp. 166-182. DOI: 10.32620/reks.2021.4.14.

25. Reji, V. and Manimegalai, C. T. V-shaped long wire frequency reconfigurable antenna for WLAN and ISM band applications. *AEU - International Journal of Electronics and Communications*, 2021, vol. 140, article id: 153937. DOI: 10.1016/j.aeue.2021.153937.

26. Prakash, T., Chaudhary, R. K. and Gangwar, R. K. Quad-Beam Octa Cross-Slotted Pattern Reconfigurable Antenna for 5.8 GHz Band Application. *2020 50th European Microwave Conference (EuMC)*, IEEE, Utrecht, Netherlands, 2021, pp. 710-713. DOI: 10.23919/EuMC48046.2021.9338028.

27. Roseli, W. I., Ali, M. T., Abd Rahman, N. H., Aris, M. A. and Yon, H. Performance Enhancement of Polarization Reconfigurable Antenna for Wireless Communication Applications. *2019 International Symposium on Antennas and Propagation (ISAP)*, IEEE, China, 2019, pp. 1-4.

28. Anantha, B., Merugu, L. and Rao, S. P. V. D. Polarization reconfigurable corner truncated square microstrip array antenna. *IETE Journal of Research*, 2021, vol. 67, iss. 4, pp. 491-498. DOI: 10.1080/03772063.2018.1557084.

29. Tran, H. H., Bui, C. D., Nguyen-Trong, N. and Nguyen, T. K. A Wideband Non-Uniform Metasurface-Based Circularly Polarized Reconfigurable Antenna. *IEEE Access*, 2021, vol. 9, pp. 42325-42332. DOI: 10.1109/ACCESS.2021.3066182.

30. Gunamony, S. L., Bala, G. J., Raj, S. M. G. and Pratap, C. B. Asymmetric coplanar strip-fed electrically small reconfigurable 5G mid-band antenna. *International Journal of Communication Systems*, 2021, vol. 34, iss. 15, article id: e4953. DOI: 10.1002/dac.4935.

Надійшла до редакції 01.10.2022, розглянута на редколегії 20.02.2023

**РЕКОНФІГУРОВАНА КОМПОЗИТНА ПРАВО/ЛІВОСТОРОННЯ ЛІНІЙНА АНТЕНА
ГІЛЬБЕРТА/МІНКОВСЬКОГО ЗІ СТУПІНЧАСТИМ ОПОРОМ
ДЛЯ БЕЗДРОТОВИХ ЗАСТОСУВАНЬ**

*Марва М. Ісмаїл, Таха А. Елві,
Алі Дж. Салім*

Предметом статті є аналіз і проектування наскрізної антени з вільного метаматеріалу на основі структури композитної правої/лівосторонньої лінії передачі (CRLH-TL). **Мета** полягає в тому, щоб розробити антену з високим коефіцієнтом підсилення з дводіапазонним резонансом, здатну змінювати свою резонансну частоту та адаптивне підсилення. **Завданнями**, які вирішуються, є створення антени з високим добутком підсилення на ширину смуги по керованих діапазонах; досягнення адаптивної реконфігурації частоти та створення прямого процесу модуляції антени за допомогою активних елементів. Використані **методи**. Пропонована антена розроблена шляхом інтеграції структури CRLH-TL до одновимірної решітки на основі двох типів елементарних комірок: перша елементарна комірка реалізована за кривою Гільберта 3-го порядку, а друга – на основі ступінчастого імпедансного резонатора (SIR) Мінковського 1-го порядку. Деталі антени надруковані на підкладці Taconic RF-43 товщиною 1,57 мм. Були отримані наступні **результати**: антена Гільберта/Мінковського–SIR досягла дводіапазонної роботи з максимальним підсиленням, рівним 14 дБі та 18 дБі на 5 ГГц та 5,5 ГГц відповідно. Крім того, змінюючи стани PIN-діода, досягається процес прямої модуляції антени зміщенням амплітуди; наприклад, на частоті 5 ГГц антена може змінювати підсилення безпосередньо в діапазоні (12-14) дБі з хорошим узгодженням імпедансу. Нарешті, запропонована антена демонструє низький профіль і працює в різних діапазонах частот нижче 6 ГГц. **Висновки**. Результати моделювання вказують на те, що таке покращення характеристик антени є результатом усунення втрат через провідність, втрат ємності на площині заземлення та усунення відбиття поверхневої хвилі завдяки введенню SIR Гільберта/Мінковського.

Ключові слова: Частотна реконфігурація; Гільберт; Мінковський; метаматеріал; SIR.

Марва М. Ісмаїл – асп. каф. електротехніки та електроніки, Технологічний університет, Багдад, Ірак.

Таха А. Елві – PhD комунікаційної техніки, доцент, зав. каф. комунікаційної техніки, коледж університету Аль-Ма Мун, Багдад, Ірак.

Алі Дж. Салім – PhD електроніки та комунікаційної техніки, доц., наук. співроб. каф. комунікаційної техніки, Технологічний університет, Багдад, Ірак.

Marwa M. Ismail – PhD student of Electrical and Electronic Department, University of Technology, Baghdad, Iraq,
e-mail: eee.19.06@grad.uotechnology.edu.iq, ORCID: 0000-0003-0510-4899, Scopus Author ID: 57215034651.

Taha A. Elwi – PhD in Communication Engineering, Assistant Professor, Head of Communication Engineering Department, Al-Ma'moon University College, Baghdad, Iraq,
e-mail: taelwi82@gmail.com, ORCID: 0000-0002-8389-5457, Scopus Author ID: 26643969700.

Ali J. Salim – PhD in Electronic and Communication Engineering, Assistant Professor, Scientific Assistant of Communications Engineering Department, University of Technology, Baghdad, Iraq,
e-mail: 30087@uotechnology.edu.iq, ORCID: 0000-0003-3185-5063, Scopus Author ID: 55083700600.